J. Opt. Fiber. Commun. Rep. 1, 84–105 (2004)

DOI: 10.1007/s10297-004-0010-4
Editors: Curtis R. Menyuk, Andrea Galtarossa

JOURNAL OF
Optical and Fiber
Communications Reports

PMD measurement techniques and how to avoid the pitfalls

Paul Williams

National Institute of Standards and Technology
Optical Fiber and Components Group
Optoelectronics Division
325 Broadway, Boulder, CO 80305 USA
Email: pwilliam@boulder.nist.gov

Abstract. Since polarization-mode dispersion (PMD) can often be so confusing, it is easy to see how its measurement can be complicated as well. Many different techniques for PMD measurement are available, and often many user-selectable parameters are associated with each measurement. Provided here is a description of the various measurement techniques available along with a discussion of the "best practices" for PMD measurement using these described techniques. Section 1 gives some definitions and lists the parameters that must be measured to fully characterize PMD and introduces the statistical uncertainty inherent in polarization-mode coupled devices. Section 2 describes the various measurement techniques, classifying them as either frequency-domain or time-domain techniques. Section 3 lists several useful practices to reduce measurement errors when measuring PMD. Section 4 discusses the concept of spectral efficiency as a useful figure of merit for describing measurement uncertainty normalized to spectral bandwidth. Finally, Section 5 describes the tradeoffs associated with wavelength step size (for frequency-domain techniques) and provides some "rules-of-thumb" for choosing appropriate wavelength steps in these measurements.

1. What Does it Take to Describe PMD?

1.1. Measurement Parameters

The PMD of a device is completely described when the Differential Group Delay (DGD) and the Principal States of Polarization (PSP) are characterized as functions of wavelength. Often, the terms PMD and DGD are used interchangeably, but here we

will use the term PMD to describe the phenomenon and DGD to describe its magnitude. Both the DGD and the PSP are contained in the three-dimensional polarization dispersion vector $\boldsymbol{\Omega}(\lambda)$. The DGD is given by the magnitude $\Delta\tau = \mid \boldsymbol{\Omega} \mid$, and the PSP are given by the direction of $\boldsymbol{\Omega}$. For many applications, only $\Delta\tau(\lambda)$ is needed, and often even the wavelength dependence is not reported, in which case PMD is described by the wavelength-averaged DGD $\langle\Delta\tau\rangle_\lambda$ or the root-mean-square (RMS) average $\langle\Delta\tau^2\rangle_\lambda^{1/2}$.

In describing the various measurement techniques, we will discuss the two general cases of PMD-devices with and without polarization-mode coupling. A "non-mode-coupled" device is a simple birefringent element such as a single birefringent crystal. In this case, the polarization eigenaxes of the device coincide with the PSP and are independent of wavelength, and $\Delta\tau$ depends only weakly on wavelength. For example, in quartz, $\Delta\tau$ changes by less than 3% over a 1300–1800 nm wavelength range (Fig. 1) [1]. In "mode-coupled" devices (such as optical fiber), the eigenaxes do not necessarily coincide with the PSPs. The PSPs are independent of wavelength only to first order, and $\Delta\tau$ can be strongly dependent on wavelength (Fig. 2).

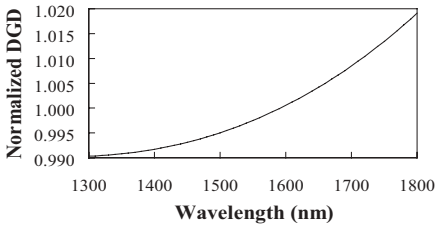

Fig. 1. Normalized DGD spectrum for quartz.

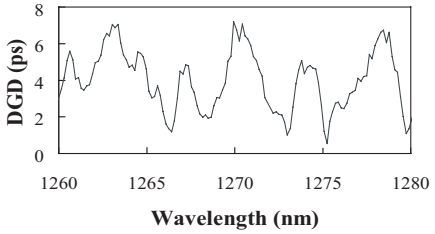

Fig. 2. Sample DGD spectrum of a mode-coupled device.

Exactly what must be measured in order to characterize the PMD of a device depends on the degree of mode coupling of the device and on what the measurement will be used for. Often, for non-mode-coupled devices, the mean DGD is well-approximated by the DGD at some particular wavelength λ_0, $\langle\Delta\tau\rangle \approx \Delta\tau(\lambda_0)$, and so the DGD need not be resolved as a function of wavelength. On the other hand, for mode-coupled devices, such as long lengths of fiber, $\langle\Delta\tau\rangle$ and $\Delta\tau(\lambda)$ can be very different. However, if only the average behavior of the device is of concern, then the mean (or RMS) DGD may suffice.

1.2. Inherent Uncertainty

A useful measurement of PMD must also report its uncertainty. Uncertainty comes not only from equipment inaccuracy, but from the environmental stability of the PMD itself. In highly mode-coupled fibers, the DGD can vary greatly with wavelength, or as temperature, stress, fiber position, or other environmental parameters change. Long, mode-coupled fiber exhibits a Maxwellian distribution of its DGD as the fiber is changed by these environmental parameters. Therefore, regardless of the quality of a measurement technique, there is an inherent uncertainty associated with measurements of DGD. So, in order to accurately report the mean DGD of a mode-coupled device, it is necessary to also report the uncertainty due to this variance of $\Delta\tau$. Gisin et al. have demonstrated that four major classes of PMD measurement techniques are subject to the same level of uncertainty due to this statistical variation of the DGD in mode-coupled devices [2]. Since all techniques essentially measure DGD (with different spectral resolutions), this variance applies to all techniques. If a fiber of mean DGD $\langle\Delta\tau\rangle$ is measured over a bandwidth of $\Delta\omega_{\mathrm{span}}$, then the standard deviation σ, normalized to $\langle\Delta\tau\rangle$, is given by [2]

$$\frac{\sigma}{\langle\Delta\tau\rangle} \approx \frac{0.9}{\sqrt{\langle\Delta\tau\rangle\Delta\omega_{\mathrm{span}}}}. \tag{1}$$

For highly mode-coupled devices, $\sigma/\langle\Delta\tau\rangle$ decreases when the average is made over a wider spectral bandwidth (or equivalently over more statistically independent samples) or when measuring a device with a larger mean DGD.

2. Measurement Techniques

The various measurement techniques can be classified as either time-domain or frequency-domain techniques. The clearest separation between the two is seen in the relationship between the coherence time T_c of the measurement light and $\Delta\tau$ (the DGD being measured). A technique is considered to be in the time domain if $T_c < \Delta\tau$, and in the frequency domain if $T_c > \Delta\tau$. Following are brief descriptions of the unique aspects of the major measurement techniques. Useful descriptions can also be found in [3].

2.1. Time-Domain Measurements

Time-of-flight Technique

The time-of-flight measurement is the most intuitive, so we consider it first. Figure 3 illustrates narrow pulses of light transmitted through a non-mode-coupled device of DGD $\Delta\tau = \tau_s - \tau_f$. The propagation delay through the device will be either τ_f (if the input pulse is polarized along the fast PSP), or τ_s (if it is polarized along the slow PSP); or if the polarization state of the pulse lies between the fast and slow PSP, the pulse will be broken into two pulses with delays τ_f and τ_s and relative intensities weighted according to the projection of the input polarization state on the PSP. So, in this intuitive measurement technique, short optical pulses are launched into a test

device and detected at the output. A fast oscilloscope plots the arrival time of the pulses as the input polarization state is changed. For launch polarizations between the two PSP of non-mode-coupled devices, two received pulses are seen separated in time by the mean DGD (averaged over the spectral bandwidth of the pulses). This technique is well known [4–6], but is often impractical since the pulse width limits the temporal resolution (requiring narrow pulse widths on the order of the desired DGD resolution).

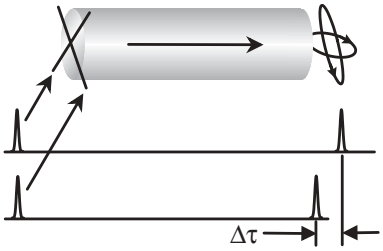

Fig. 3. Diagram of input pulses launched simultaneously down the fast and slow PSP of a device. Output pulses emerge at different times corresponding to the difference in group delay.

Low-Coherence Interferometry

A related but more practical approach to time-domain measurement is low-coherence interferometry (Fig. 4). A spectrally broad (low-coherence) source sends light through the test device and into an interferometer. As the moveable arm of the interferometer is translated, interference fringes are seen at the detector only if the time-delay difference between the two arms matches a delay generated in the test device to within the coherence time of the source. Ignoring possible phase effects, this condition can be written simplistically as

$$| \, (\tau_{\mathrm{arm},1} - \tau_{\mathrm{arm},2}) - (\tau_i - \tau_j) \, | < T_c, \tag{2}$$

where $\tau_{\mathrm{arm},1}$ and $\tau_{\mathrm{arm},2}$ are the time delays associated with propagation along each arm of the interferometer, and τ_i and τ_j are two possible propagation times experienced by light traveling along the ith and jth polarization paths through the device. T_c is the coherence time of the source (e.g., for a Gaussian source of spectral width $\Delta\lambda$ and center wavelength λ, $T_c = 0.664\lambda^2/(c\Delta\lambda)$, where c is the speed of light) [7]. Equation (2) gives an intuitive picture of the shape of the interferogram. For the non-mode-coupled case, there are only two nondegenerate paths through the device—light traveling along the fast axis or along the slow axis. So, the only possible values of the difference $\tau_i - \tau_j$ are 0 or $\pm\langle\Delta\tau\rangle_\lambda$, where $\langle\Delta\tau\rangle_\lambda$ is the result of an average of the DGD over the spectrum of the source, weighted by the intensity of the source at each wavelength.

Plotting the envelope of interference fringes as the moveable arm of the interferometer is scanned gives a delay histogram similar to Fig. 5 for a non-mode-coupled device. The central peak of the delay histogram is the autocorrelation of the source, which gives no information about the strength of the PMD ($\tau_i - \tau_j = 0$). The two side lobes are separated from the autocorrelation peak by an amount $\langle\Delta\tau\rangle_\lambda$. So, for non-mode-coupled devices, measuring the separation of the side lobes gives $2\langle\Delta\tau\rangle_\lambda$.

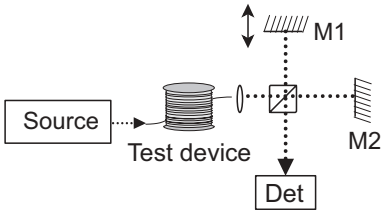

Fig. 4. Schematic diagram of low-coherence interferometer: M1 is the movable mirror.

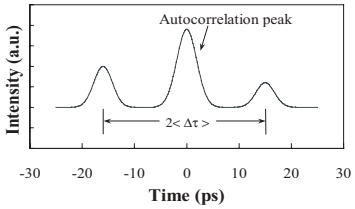

Fig. 5. Sample interferogram envelope for a non-mode coupled device.

The peak at 0 is the coherence function of the source (in the absence of chromatic dispersion or interference from the side lobes) and its width gives the source coherence time, which provides the temporal resolution limit. In other words, if the PMD is too low, the side-lobe separation will be on the order of the coherence time of the source, causing the side lobes to add coherently with the central peak and making it difficult to identify their position. This illustrates the tradeoff between bandwidth and DGD resolution; a broader source better resolves the DGD, but at the expense of the spectral resolution of the DGD.

The finite width of the side lobe peaks at $\pm\langle \Delta\tau \rangle_\lambda$ has two separate causes. First, the coherence time of the source broadens the peak. Second, if the value of $\Delta\tau$ is not constant over the source spectrum, there will be some broadening of the peak due to variation of DGD with wavelength.

Low-coherence interferometry can be used to measure mode-coupled devices as well. In this case, τ_i and τ_j in Eq. (2) can take on 2^{N+1} different values (where N is the number of mode-coupling sites in the artifact). This yields a delay histogram with 2^{N+2}-1 peaks. However, the separation of adjacent peaks can easily be less than the coherence time of the source, and so the peaks are not necessarily distinguishable. The resulting interferogram envelope comes from the coherent addition of the various delays. Figure 6 gives an example delay histogram for a highly mode-coupled device. In such devices, it is customary to characterize the RMS value of the DGD over the wavelength range of the measurement. The "second moment"

$$\sigma_M = \sqrt{\frac{\int I(t) t^2 dt}{\int I(t) dt}} \tag{3}$$

of this Gaussian-shaped delay histogram will generally[1] yield the RMS DGD value ($I(t)$ is the amplitude of the delay histogram and t is the time component). The relationship between the two is [8]

$$\langle \Delta\tau^2 \rangle^{1/2} \approx \sqrt{\frac{3}{4}}\sigma_M. \tag{4}$$

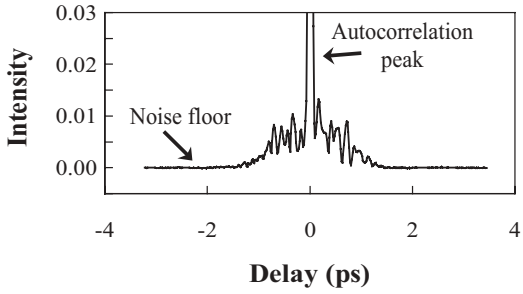

Fig. 6. Sample interferogram envelope for a mode-coupled device.

Equation (3) should be evaluated with caution. There will be non-ideal features of the delay histogram that make it deviate from a true Gaussian. The most significant features are the autocorrelation peak and the noise floor (dominant at high values of t). The integration limits for Eq. (3) must be chosen carefully in order to exclude these unwanted features, but this must be done iteratively so as not to incur a bias in the opposite direction due to excluding real data. Examples of procedures to correctly extract $\langle \Delta\tau^2 \rangle^{1/2}$ from a mode-coupled interferogram are provided in [9] and [10]. Recently, a promising approach to low-coherence interferometry was presented that uses polarimetric detection and appears to completely remove the central peak from both mode-coupled and non-mode-coupled interferograms, thus allowing the same measurement algorithm to be used regardless of the degree of mode-coupling [11].

PMD measurements using low-coherence interferometry have several advantages over other techniques. The measurements can be done quickly-the time required is essentially the travel time of the interferometer mirror over the desired scan range (a few seconds). Unlike most of the frequency—domain techniques, low-coherence interferometry does not require numerical comparison of data sampled at two different points in time. This makes interferometry less susceptible to dynamic changes in the measurement path (such as movement of the fiber leads or temperature drift). A disadvantage of low-coherence interferometry has been the need to use a spectrally broad source, which limits achievable spectral efficiency (ability to measure with fine temporal resolution in a narrow bandwidth). However, resolutions as low as 11 fs have been demonstrated using a differential technique [12], and long-haul measurements through

[1] Equation (4) assumes a large DGD-source-bandwidth product. When the magnitude of this product is small, the relationship between σ_M and the RMS DGD is a function of the exact shape of the low-coherence source [8].

multiple bandwidth-limiting optical amplifiers have demonstrated good measurement results with a bandwidth of only 20 nm [13].

Another aspect of making PMD measurements using low-coherence interferometry is the effect of multipath interference (MPI). Multiple reflections within the measurement path will cause delays in the signal transmission that are indistinguishable from delays due to PMD. While it may be useful to measure these MPI effects, the user should be aware that low-coherence interferometry does not distinguish between MPI and PMD [14,15].

2.2. Frequency-Domain Measurements

PMD measurements based in the frequency domain measure the same DGD as time-domain measurements but from a different perspective. The most common approach to DGD measurement in the frequency domain involves a differential method. The difference in propagation delay between light traveling on the fast and slow PSP determines the output polarization state $\hat{\mathbf{s}}_{\mathrm{out}}$ of the light. Frequency-domain measurements of PMD do not seek to find how the polarization state of monochromatic light is transformed as it passes through the device under test, but rather how the output polarization state changes as a function of optical frequency. In the absence of polarization-dependent loss (PDL), the polarization dispersion vector $\boldsymbol{\Omega}$ is related to this change in output state as [16]

$$\frac{d\hat{\mathbf{s}}_{\mathrm{out}}}{d\omega} = \boldsymbol{\Omega} \times \hat{\mathbf{s}}_{\mathrm{out}}, \tag{5}$$

where ω is the angular optical frequency of the light. The physical meaning of this expression is that PMD in a device causes the output polarization state to precess about $\boldsymbol{\Omega}$ as the optical frequency is changed (Fig. 7). From Eq. (5), the precession rate will be equal to the DGD of the device:

$$\left|\frac{d\theta}{d\omega}\right| = \mid \boldsymbol{\Omega} \mid = \Delta\tau, \tag{6}$$

where θ is defined in Fig. 7 as the angle of rotation of the output state of polarization about the precession axis $\boldsymbol{\Omega}$. The DGD can be found by measuring $\Delta\theta/\Delta\omega$ (as an approximation to $d\theta/d\omega$). The class of frequency-domain techniques that measure $\Delta\theta/\Delta\omega$ will be referred to as "polarimetric techniques."

The distinction between the various polarimetric techniques is how they measure $\Delta\theta/\Delta\omega$. The techniques all begin with launching polarized light into the test device and measuring the output state as a function of optical frequency, $\hat{\mathbf{s}}(\omega)$. But the change in $\hat{\mathbf{s}}$ with frequency yields $\mid \Delta\hat{\mathbf{s}}/\Delta\omega \mid$, not $\Delta\theta/\Delta\omega$, and this is where the variation in approaches comes in.

Three very similar techniques of polarimetric measurement of DGD will be discussed here-Jones Matrix Eigenanalysis (JME) [17], Müller Matrix Method (MMM) [18], and Poincaré Sphere Analysis (PSA) [19, 20]. All three offer means of assessing both $\Delta\tau$ and the PSP from the wavelength dependence of the output polarization state, and all three can be measured by use of the same experimental setup (Fig. 8).

Jones Matrix Eigenanalysis

The JME technique gives a measurement of $\Delta\theta/\Delta\omega$ and $\boldsymbol{\Omega}$ by turning the measurement into an eigenvalue problem [17]. A difference matrix $\boldsymbol{\Gamma}$ is defined as a 2×2 Jones

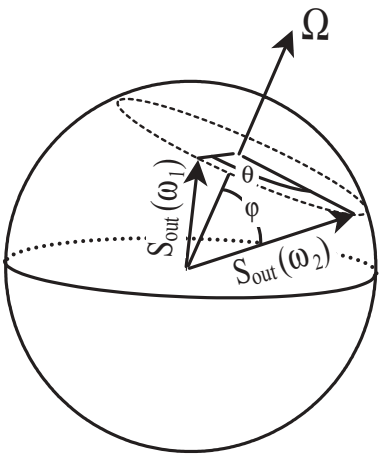

Fig. 7. Poincaré sphere representation of polarization dispersion vector $\boldsymbol{\Omega}$ and output polarization state $\hat{\mathbf{s}}_{\mathrm{out}}$ at optical frequencies ω_1 and ω_2.

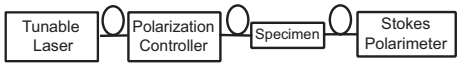

Fig. 8. General diagram of experimental setup for JME, MMM, and PSA measurement techniques.

matrix that describes the change in output polarization state as the optical frequency is changed from ω_1 to ω_2,

$$\hat{\mathbf{s}}_{\mathrm{out}}(\omega_2) = \boldsymbol{\Gamma}(\bar{\omega}, \Delta\omega)\hat{\mathbf{s}}_{\mathrm{out}}(\omega_1), \tag{7}$$

where $\bar{\omega} = (\omega_1 + \omega_2)/2$ is the average frequency and $\Delta\omega = \omega_2 - \omega_1$ is the frequency step size. It must be noted that $\boldsymbol{\Gamma}$ is not the transfer matrix of the DUT (it does not transform an input state to an output state). Instead, it describes the motion of the output state as the wavelength is changed. Equations (5) and (6) show that a change in wavelength causes the output polarization state to precess about the PSP with a rate equal to the DGD. Therefore, eigenstates of $\boldsymbol{\Gamma}$ are the PSP, and the DGD is derived from the eigenvalues.

At a given optical frequency ω_1, three noncollinear input polarization states (such as linear polarization with 0°, 45°, and 90° orientations) are input to the device and the corresponding output polarization states $\hat{\mathbf{s}}_{\mathrm{out}}$ are measured. This allows the 2×2 Jones transfer matrix $\mathbf{T}(\omega_1)$ to be calculated following [21]. $\mathbf{T}(\omega_1)$ is the matrix that describes the transformation of the input polarization state to the output polarization state at the optical frequency ω_1, $\hat{\mathbf{s}}_{\mathrm{out}}(\omega_1) = \mathbf{T}(\omega_1)\hat{\mathbf{s}}_{\mathrm{in}}$. Then the same three states are launched at a slightly different optical frequency ω_2, and $\mathbf{T}(\omega_2)$ is calculated.

We then find $\boldsymbol{\Gamma}$ as the product $\boldsymbol{\Gamma}(\bar{\omega}, \Delta\omega) = \mathbf{T}^{-1}(\omega_2)$. As mentioned above, $\boldsymbol{\Gamma}$ describes the evolution of the output polarization state as the optical frequency is changed. When no PDL is present, the output state precesses about the PSP. So, the eigenvectors of $\boldsymbol{\Gamma}$ are the PSP, and the two eigenvalues are $\rho_q = \exp(i\tau_{g,q}\Delta\omega)$, where the index q denotes propagation along the fast or slow axis and $\tau_{g,q}$ is the associated group delay. The DGD is then

$$\Delta\tau(\bar{\omega}) =\mid \tau_{g,s} - \tau_{g,f} \mid= \left|\frac{\mathrm{Arg}(\rho_s/\rho_f)}{\Delta\omega}\right|. \tag{8}$$

Thus, JME allows the full $\boldsymbol{\Omega}(\bar{\omega})$ to be calculated, even for highly mode-coupled devices. The matrix $\boldsymbol{\Gamma}$ is found with complete generality and is correct even in the presence of PDL. However, when PDL is present, the eigenstates of $\boldsymbol{\Gamma}$ will be nonorthogonal, and the expression for DGD, Eq. (8), will no longer be exact.

Müller Matrix Method

The Müller Matrix Method (MMM) [18] measures PMD in much the same way as the JME technique, but with two slight differences. First, their calculations are carried out in different vector spaces (MMM uses Müller matrices, but JME uses Jones matrices). This simplifies the algorithm for the MMM case. Second, the entire MMM measurement assumes the absence of PDL, contrary to JME, where the absence of PDL is assumed only in the last step (as the DGD is calculated). This allows MMM to determine the difference matrix by launching only two polarization states per wavelength (as opposed to three for JME) and yields a difference matrix that describes a pure rotation θ of the output state with wavelength. The rotation angle θ substituted in Eq. (6) yields the DGD, and the rotation axis is the PSP. The tradeoff is that the JME difference matrix $\boldsymbol{\Gamma}$ is exact even in the presence of PDL, while the MMM difference matrix $\mathbf{R}_\Delta$ is not. This makes JME less susceptible than MMM to the presence of PDL. This can be demonstrated by simulation [22].

MMM first measures the Müller transfer matrix $\mathbf{R}$ for optical frequencies ω_1 and ω_2. By assuming no PDL, a 3×3 reduced Müller matrix describing $\mathbf{R}$ can be found by measuring the output state for only two input states. These two states can simply be two different linear polarizations (the angle between them is not important to the measured value, but will have an effect on the measurement noise).

The MMM technique measures the polarization transfer matrix $\mathbf{R}$ at two closely spaced optical frequencies, yielding $\mathbf{R}(\omega_1)$ and $\mathbf{R}(\omega_2)$, and calculates the difference matrix as $\mathbf{R}_\Delta = \mathbf{R}(\omega_2)\mathbf{R}^T(\omega_1)$, which describes the change in output polarization state as the optical frequency is changed from ω_1 to ω_2. In the absence of PDL, $\mathbf{R}_\Delta$ corresponds exactly to $\boldsymbol{\Gamma}$ in JME, and $\mathbf{R}$ and $\mathbf{R}_\Delta$ are pure rotation matrices, which means $\mathbf{R}^T = \mathbf{R}^{-1}$. Since $\mathbf{R}_\Delta$ is a rotation matrix, the precession angle θ of the output polarization state about $\boldsymbol{\Omega}$ is given by

$$\cos(\theta) = \frac{1}{2}(\mathrm{Tr}\mathbf{R}_\Delta - 1), \tag{9}$$

where $\mathrm{Tr}\mathbf{R}_\Delta$ is the trace of $\mathbf{R}_\Delta$. This is used in Eq. (6) to yield the DGD. The PSP is the rotation axis, and is found as the eigenvector of $\mathbf{R}_\Delta$ that corresponds to an eigenvalue of 1 [23]. This is detailed in [18].

Poincaré Sphere Analysis

The Poincaré Sphere Analysis (PSA) technique is closely related to both JME and MMM. In fact, the same measurement procedures can be used for both JME and PSA measurements; only the data analysis differs. As with MMM, PSA analysis takes place entirely in Stokes space, and assumes the absence of PDL throughout the process.

The PSA technique works with frequency derivatives of the measured output Stokes vectors rather than derivatives of the polarization transfer matrix (which JME and MMM effectively do). The relationship between the output polarization states and the PMD is as follows. Consider three output states $\hat{\mathbf{h}}$, $\hat{\mathbf{q}}$, and $\hat{\mathbf{c}}$, which are orthogonal on the Poincaré sphere. An infinitesimal change of optical frequency $d\omega$ will rotate these states through an angle $d\theta$ on the Poincaré sphere, causing changes in these states of $d\hat{\mathbf{h}}$, $d\hat{\mathbf{q}}$, and $d\hat{\mathbf{c}}$, respectively. Geometrically, the relationship between the motion of the states and the rotation angle is

$$d\theta = \sqrt{\frac{(d\hat{\mathbf{h}})^2 + (d\hat{\mathbf{q}})^2 + (d\hat{\mathbf{c}})^2}{2}}. \tag{10}$$

However, for a finite change $\Delta\omega$ in optical frequency, an approximation must be used to give a more accurate expression for $\Delta\theta$. Combining this with Eq. (6) relates the finite changes in the three orthogonal output states to the DGD as

$$\Delta\tau = \left|\frac{\Delta\theta}{\Delta\omega}\right| = \frac{2}{\Delta\omega}\arcsin\left(\frac{1}{2}\sqrt{\frac{1}{2}(\Delta\mathbf{h}^2 + \Delta\mathbf{q}^2 + \Delta\mathbf{c}^2)}\right). \tag{11}$$

The PSP is also found geometrically as the axis about which $\hat{\mathbf{h}}$, $\hat{\mathbf{q}}$, and $\hat{\mathbf{c}}$ rotate:

$$\text{PSP} = \frac{\boldsymbol{\Omega}}{|\,\boldsymbol{\Omega}\,|} = \frac{\mathbf{u}}{|\,\mathbf{u}\,|}, \tag{12}$$

with $\mathbf{u} = (\mathbf{c}\cdot\Delta\mathbf{q})\mathbf{h} + (\mathbf{h}\cdot\Delta\mathbf{c})\mathbf{q} + (\mathbf{q}\cdot\Delta\mathbf{h})\mathbf{c}$.

The PSA technique finds $\hat{\mathbf{h}}$, $\hat{\mathbf{q}}$, and $\hat{\mathbf{c}}$ at two closely spaced optical frequencies, then calculates $d\hat{\mathbf{h}}$, $d\hat{\mathbf{q}}$, and $d\hat{\mathbf{c}}$ and uses Eqs. (11) and (12) to find the PMD. A variety of methods may be used, but a simple approach is to launch two linear polarization states separated by approximately 90° on the Poincaré sphere (e.g., horizontal and vertical polarizations). In the absence of PDL, the corresponding output states $\hat{\mathbf{h}}'$, and $\hat{\mathbf{q}}'$ will have the same angle between them as the input states. For nonorthogonal launch states, corrected orthogonal output states are generated as $\hat{\mathbf{h}} = \hat{\mathbf{h}}'$ and

$$\hat{\mathbf{q}} = (\hat{\mathbf{h}} \times \hat{\mathbf{q}}') \times \hat{\mathbf{h}} / \,|\, \hat{\mathbf{h}} \times \hat{\mathbf{q}}' \,|\,.$$

The third mutually orthogonal state is generated as $\hat{\mathbf{c}} = \hat{\mathbf{h}} \times \hat{\mathbf{q}}$.

PA, SOP, and PS Techniques

Various other polarimetric measurement techniques with similarities to JME, PSA, and MMM are sometimes mentioned. However, their names generally come up under the topic of "Other measurement techniques." These techniques, Poincaré Arc (PA), State of Polarization (SOP) and Poincaré Sphere (PS), are often mentioned without literature references, and so it is difficult to define a measurement procedure to associate with each name. A good generalization would be to use these somewhat generic titles to refer to techniques that measure the DGD by measuring only $\hat{\mathbf{s}}_{\text{out}}/\Delta\omega$. This requires the assumption that

$$\left|\frac{d\hat{\mathbf{s}}_{\text{out}}}{d\omega}\right| = \left|\frac{d\theta}{d\omega}\right|. \tag{13}$$

This is true when $\hat{\mathbf{s}}_{\mathrm{out}}(\omega)$ lies on a great circle, and occurs when an input polarization state is launched so that both PSP are equally illuminated. This condition is difficult to maintain in a mode-coupled device such as a long fiber, but is possible in non-mode-coupled components.

Fixed-Analyzer Technique

The fixed-analyzer (FA) technique [24] offers a simplified approach to a polarimetric measurement. It is sometimes called wavelength scanning. The FA technique measures mean DGD based on Eq. (6), but indirectly. Figure 9 illustrates the basic setup. Light transmitted through a polarizer–test device–polarizer setup is detected as a function of wavelength. This can be done either with a tunable laser and detector combination or with a broadband source and an optical spectrum analyzer (or monochromator). As the output polarization vector $\hat{\mathbf{s}}_{\mathrm{out}}(\omega)$ moves around the sphere, the normalized intensity $I_N(\omega)$ transmitted through the output polarizer of Fig. 9 is given as

$$I_N(\omega) = \frac{1}{2}(1 + \sin\Phi\cos[\theta(\omega)]\sin\varphi + \cos\Phi\cos\varphi), \tag{14}$$

where the angles are in Poincaré sphere coordinates, Φ is the angle between $\boldsymbol{\Omega}$ and the Stokes vector describing the transmission axis of the output polarizer, and φ is the angle between $\mathbf{s}_{\mathrm{out}}$ and $\boldsymbol{\Omega}$ (Fig. 7). Φ and φ are independent of ω for non-mode-coupled devices. $\theta(\omega)$ is the azimuthal angle of the precession of $\hat{\mathbf{s}}_{\mathrm{out}}(\omega)$ about $\boldsymbol{\Omega}$. For non-mode-coupled devices, $\theta(\omega)$ depends approximately linearly on ω and contains all of the optical frequency dependence of $I_N(\omega)$. So we can estimate $d\theta/d\omega$ (and thus average DGD $\langle\Delta\tau\rangle$) from Eq. (6) by merely counting the number of extrema (peaks and valleys) in the sinusoidal $I_N(\omega)$ curve over a given optical frequency range. That is,

$$\langle\Delta\tau\rangle_{\omega_a-\omega_b} = \frac{kN_e\pi}{\omega_b - \omega_a} = \frac{kN_e\lambda_a\lambda_b}{2(\lambda_a - \lambda_b)c}, \tag{15}$$

where the brackets indicate the average DGD measured over the frequency range from ω_a to ω_b, k is a mode-coupling constant (equal to 1 for non-mode-coupled devices), and N_e is the number of peaks and valleys measured over the frequency range from ω_a to ω_b. The right-most expression in Eq. (15) is merely the same expression as the middle one, but given in terms of wavelength instead of optical frequency.

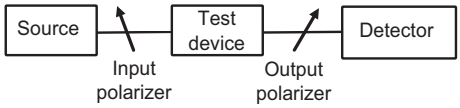

Fig. 9. Diagram of fixed analyzer setup.

If we consider the case of a mode-coupled device, the situation becomes more complicated in that $d\theta/d\omega$ can depend strongly on ω, and $\boldsymbol{\Omega}$ can also have a second-order dependence on ω ($\boldsymbol{\Omega}$ is still independent of ω to first order). This means that $I_N(\omega)$ no longer has a simple sinusoidal dependence but behaves in a quasi-random way as shown in Fig. 10. Fortunately, the mean DGD can still be estimated by counting peaks and valleys in the $I_N(\omega)$ spectrum. In this case, the coupling factor k becomes

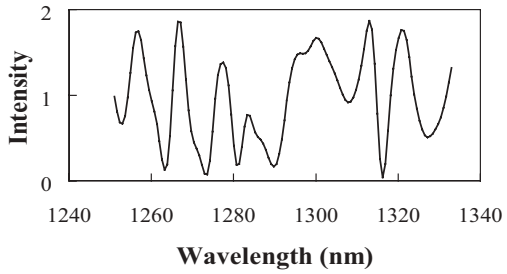

Fig. 10. Typical spectrum from fixed analyzer measurement of non-mode-coupled device.

0.805. k comes from a Monte Carlo simulation and allows mean DGD to be accurately estimated when the device is strongly mode-coupled [25].

Evaluating the mean DGD from $I_N(\omega)$ is straightforward for a non-mode-coupled device since it merely involves counting peaks and valleys of a sinusoidal signal. However, in the case of mode-coupled devices, it can become difficult to distinguish peaks and valleys from intensity noise. Often a "thresholding" algorithm is used to ignore peaks and valleys whose extent is less than some defined fraction of the full-scale excursion of $I_N(\omega)$. This practice will incur a bias due to ignoring some fraction of real peaks and can easily give errors of $\sim 10\%$. This problem is discussed in [25] and there a lookup-table correction factor is suggested to reduce this bias. FA measurements on mode-coupled devices can also be biased by sampling too coarsely (causing small peaks to be missed, thus underestimating the mean DGD). In order to sample $I_N(\omega)$ sufficiently, a device of nominal mean DGD $\langle \Delta\tau \rangle$ should be measured with at least $2\langle \Delta\tau \rangle \Delta\omega$ frequency points for a measurement spectrum of $\Delta\omega$ [25].

An alternative evaluation of the FA spectral data is often used. Rather than calculating $\langle \Delta\tau \rangle$ from an estimate of $d\theta/d\omega$ based on counting peaks and valleys, the $I_N(\omega)$ spectrum can be Fourier-transformed into the time domain. The result is a "delay histogram" very similar to that which would be seen for a low-coherence interferometric measurement with the same source spectrum as used in the FA measurement (windowing is often used to optimize the results). The mean DGD can then be evaluated in the time domain by the same means as with low-coherence interferometry [26].

RF Phase Shift Technique

This technique resembles the time-of-flight measurement. Figure 11 illustrates a typical setup. A tunable laser is intensity-modulated at a frequency ranging from several tens of megahertz to a few gigahertz. The modulated light passes through a polarization controller, then the test device, and then is detected. The RF phase φ_{RF} of the detected signal is referenced to the phase of the modulator as the polarization state of the light is changed. φ_{RF} is related to the time of flight through the device, so that as the input polarization state is changed, the maximum and minimum phases $\varphi_{\mathrm{RF,max}}$ and $\varphi_{\mathrm{RF,min}}$, can be measured and used to find the maximum and minimum polarization-dependent propagation delays through the device. Their difference gives the DGD through the test device,

$$\Delta\tau = \frac{\varphi_{\mathrm{RF,max}} - \varphi_{\mathrm{RF,min}}}{360^\circ \cdot f_{\mathrm{mod}}}, \tag{16}$$

where phases are given in degrees and f_{mod} is the RF modulation frequency [27].

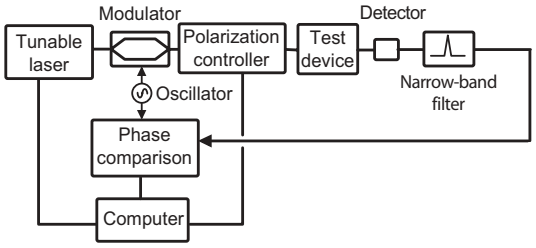

Fig. 11. Generic diagram of experimental setup for RF phase shift measurement system.

The down-side of this intuitive randomized-launch approach is that to accurately find the maximum and minimum requires many phase measurements while the polarization state is randomly varied. Over this measurement time, noise or drift in RF phase will generally increase the difference between $\varphi_{\mathrm{RF,max}}$ and $\varphi_{\mathrm{RF,min}}$, biasing the results toward larger DGD values. Thus, environmental drift in the optical path length of the DUT can cause significant systematic measurement errors.

This approach is improved by algorithms that allow $\Delta\tau$ and the PSP to be obtained by measuring the RF phase at just four known polarization states (launched at points orthogonal to each other on the Poincaré sphere). Two such implementations are the Modulation Phase Shift (MPS) technique [28] and Polarization-dependent Signal Delay (PSD) method [29]. By minimizing the number of phase measurements, the measurement time and resulting errors due to drift of the optical path length are significantly reduced. It has also been shown that by launching six states instead of only four, improved stability against drift can be gained [30].

RF phase shift is a promising technique in that it allows one to make narrowband measurements whose spectral width is due only to the RF modulation frequency. The classification of the RF phase-shift techniques as frequency-domain is somewhat ambiguous. The definition of time and frequency domains generally relies on the coherence length of the optical source, but in principle the MPS and PSD techniques will work with either a spectrally narrow laser source or a broadband source (though the latter negates the narrow-bandwidth advantages of RF phase-shift measurements). The choice to include RF techniques in the frequency domain is therefore based on the coherence time of the RF modulation.

Swept-wavelength Interferometry

Recently, a new class of measurement technique has been developed that finds PMD from measurement of the full optical transfer function of the DUT [31]. The "swept-wavelength interferometer" technique uses a dual Mach-Zehnder interferometer configuration with a frequency-swept laser as the source. As shown in Fig. 12, interferometers at both the input and output of the DUT enable characterization of the full magnitude and optical phase of light reflected and transmitted by the DUT. A polarization-delay element delays one polarization state of the launched light with respect to its

orthogonal state. Since the source wavelength is time dependent, at a given time the two orthogonal polarization states are at different optical frequencies, causing each of the two launched polarization states to generate a different beat frequency at the detector. Filtering this frequency allows simultaneous distinguishable measurements of the two launched polarization states. Thus, the system yields the polarization-dependent magnitude and optical phase for transmission and reflection, allowing calculation of the polarization-dependent transmission and reflection matrices of the DUT at each optical frequency as the laser is swept. The data can be post-processed to measure the DGD and PSP with a variable spectral resolution (trading temporal resolution for frequency resolution).

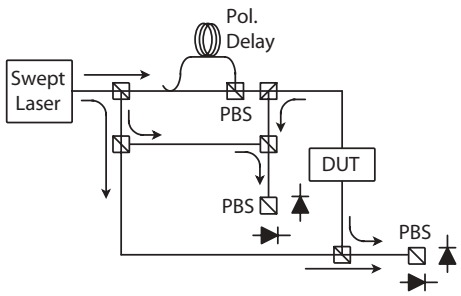

Fig. 12. Schematic of swept-wavelength interferometer. Arrows indicate light direction and PBS is a polarizing beam splitter.

This technique is attractive because of its speed and versatility, allowing it to simultaneously measure DGD, group delay, insertion loss, and polarization-dependent loss. It is also capable of simultaneous measurement of multiport components [32]. Full-scan periods are on the order of one minute. A limitation of this technique is that the source coherence limits the optical path length of the DUT to several tens of meters, making the technique unsuitable for long fibers.

3. Experimental Setup Details

Once a measurement technique is chosen, there are several precautions to be taken in making PMD measurements. Some of the most important are detailed below.

3.1. Inherent Lead PMD

When PMD is measured, it is important that there be minimal stray PMD in the measurement system or the fiber leads. The leads connecting the measurement system to the device being tested can have inherent birefringence (due to asymmetries or stresses from the manufacturing process), which leads to PMD. The DGD due to these stresses will be a few femtoseconds for lead lengths of a few meters. Selection of low-PMD leads and use of the shortest lengths possible will minimize errors due to lead birefringence.

3.2. Bend-induced PMD in Leads

Even low-PMD leads can exhibit significant PMD under bending, which causes a stress-induced birefringence. The bend-birefringence increases as $1/r^2$, where r is the radius of the fiber bend [33]. Extending this to DGD, we find the bend-induced DGD varies as $1/r$. Measurements should be made with the fiber leads as short and as straight as possible.

Once lead PMD has been minimized, it is best to measure the remaining PMD of the measurement system by removing the test device, connecting the leads together and measuring the "instrument DGD." Since PMD is a vector quantity, the device DGD and the instrument DGD will not simply add as scalars, but as vectors. The combined DGD will depend on the relative orientations between the PSP axis within the leads and the PSP axis of the test device. In other words, the final measurement cannot be corrected by simply subtracting the measured value for instrument DGD. The best solution is to measure the device several times with the leads re-oriented in between each measurement (avoiding small bend radii). The average of these multiple measurements will give the best estimate of the device DGD, and the spread in the measured values will be an estimate of the instrument DGD. The final value will still have effects due to instrument birefringence; but, they can be documented by including the instrument DGD in the uncertainty statement for the device.

3.3. Stabilizing the Measurement

Care should be taken before the measurement to stabilize both the measurement system and the test device against temperature changes or movement. Even fiber leads having only a small amount of DGD can have a big effect on measurement noise if they are moving during the measurement. This is particularly important for the polarimetric measurement techniques, which measure the output polarization state of the light in order to determine the DGD. A moving fiber lead can change the output polarization state significantly, resulting in a time-dependent output polarization state. When the polarization state is measured at different wavelengths, this effect of lead motion will falsely be identified as a change in polarization state with wavelength (DGD). The resulting DGD error will be proportional to the total DGD being measured (not just the DGD of the leads). Given the random nature of lead motion, this DGD error is likely to also be random, but could have an amplitude large enough to obscure the true DGD.

For MPS and PSD techniques, where the measured DGD comes from four measurements separated in time from each other, moving fiber leads at the input of the DUT can cause errors proportional to the total DGD. In the case of low-coherence interferometry, the polarization state is not directly measured, and the light propagating down different polarization states of the test device is detected simultaneously, so there is much less effect from moving fiber leads. In general, for all measurements, it is best to secure the fiber leads against motion during measurements.

Temperature should also be kept stable during a measurement—even for devices with relatively low temperature dependence of their DGD. The reason for this is the same as with the moving fiber leads. A change in temperature of the device will change the birefringence slightly, causing the polarization state to change with time, which produces a DGD error proportional to the total DGD of the measurement.

Generally, temperature drift is of greater concern, since as the temperature increases, the output polarization state will precess about the eigenaxis of the DUT. This means that drifting temperature will systematically bias the measured DGD (the sign of this bias is determined by the direction of the temperature drift), as opposed to the random error due to lead motion.

Figure 13 shows an example of DGD error due to temperature drift. Here, a simple quartz plate element was measured as the temperature changed from room temperature to $\sim 40^{\circ}$C in about 30 min. From the graph, it is clear that when the temperature is stable, there is little difference between the DGD measured at room temperature and at the elevated temperature (the quartz plate shows a temperature coefficient of approximately 0.08 fs/$^{\circ}$C). However, during the transition between room temperature and the elevated temperature, the DGD varied significantly. This illustrates the importance of a stable temperature environment for the measurement. It should be noted that in this example, the error appears to be random with time. This is attributable to the extreme change of temperature with time causing the polarization state to rotate on the sphere at a rate faster than the sampling time of the measurement, randomizing the sign of the bias. For slower temperature changes, a more systematic bias is observed.

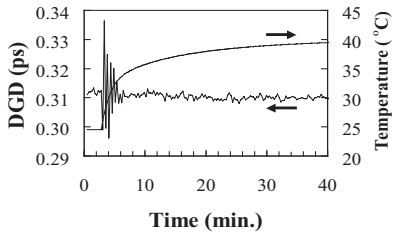

Fig. 13. Measured DGD versus time for a quartz plate as the temperature is changed as shown.

Since the magnitude of DGD error incurred by temperature drift is proportional to the rate of change of temperature, it is best if devices can be held at a constant temperature or at least insulated to allow any temperature changes to occur only slowly. Effects of temperature drift can also be reduced by careful choice of sampling order. DGD bias comes when a drifting polarization state is falsely assumed to come from the changing wavelength. This systematic bias could be randomized by sampling wavelength points in a random order, where the wavelength change is not always in the same direction. Or, when the temperature drift is linear, the problem can be virtually eliminated by measuring the polarization state (in the case of polarimetric techniques) at wavelengths λ_1, λ_2, and then at λ_1 again, and averaging the results for the two λ_1 measurements, effectively obtaining λ_1 and λ_2 measurements at the same drift position of the polarization state. This approach also works well for RF phase-shift measurements.

Again, it is expected that this effect on the DGD will be greater for frequency-domain measurements and less for interferometric measurements.

3.4. Multipath Interference

When multiple reflections occur within the measurement path, a cavity is set up where a fraction of the light passing through the cavity makes more than one pass, receiving extra delay. This will show up on an interferometric measurement and be indistinguishable from DGD. This will also show up as a ripple on FA spectra (in the absence of source normalization) that could be mistaken for higher DGD values. In the rest of the frequency-domain measurements, the measured DGD will not be affected by multiple reflections unless the cavity contains DGD. In that case, the DGD spectrum will have a ripple whose amplitude depends on the amount of DGD within the cavity and on the strength of the reflections [14]. The period of these multiple-reflection-induced ripples will come from the cavity spacing. When there is DGD in the cavity, there will be two spacings—one associated with the fast PSP and the other with the slow PSP. These two closely spaced periodicities will result in a fast ripple with a slow envelope modulation. The fast ripple will repeat with an angular frequency spacing of

$$\Delta\omega_0 = \frac{\pi c}{L n_g}, \tag{17}$$

and the beat note envelope will have a frequency spacing of

$$\Delta\omega_B = \frac{\pi c}{L \Delta n_g}, \tag{18}$$

where L is the physical length of the cavity, n_g is the group index and Δn_g is the group birefringence of the cavity [15].

When multipath interference is measured, it is important to be aware of the source and implications of the interference. Interferometry and un-normalized fixed-analyzer techniques do not distinguish between polarization-dependent and -independent multipath interference. This is important if general dispersion is the concern. On the other hand, polarimetric techniques report only polarization-dependent multipath interference. This is useful when only polarization-dependent dispersion is important (e.g., in polarimetric DGD compensation).

4. Spectral Efficiency

In all methods of DGD measurement, there is a trade-off between the spectral bandwidth used to make the measurement and the achievable DGD resolution. The bandwidth efficiency factor α_B relates the achievable signal-to-noise ratio (SNR) to the DGD-bandwidth product as

$$\alpha_B = \left(\frac{\mathrm{SNR}}{\Delta\omega}\right)\frac{1}{\Delta\tau}, \tag{19}$$

where $\Delta\tau$ is the DGD of the device and $\Delta\omega$ is the angular frequency spectrum used by the measurement (i.e., the measurement bandwidth). α_B can be thought of as the achievable SNR per bandwidth normalized to the mean DGD. α_B depends on the particular measurement technique and the quality of the equipment. Equation (19) illustrates that for a given measurement (fixed α_B), the SNR can be improved by

increasing the measurement bandwidth. Or, when the measurement bandwidth is fixed, the SNR improves when measuring larger DGDs. Expressing SNR as $\Delta\tau/\sigma$, where σ is the measurement standard deviation, we can also write the efficiency factor as

$$\alpha_B = \frac{1}{\sigma \cdot \Delta\omega}. \tag{20}$$

This useful form makes calculation of α_B simple. The bandwidth efficiency is a useful figure of merit for measuring narrowband components. It describes the relationship between DGD uncertainty and spectral resolution. When comparing the performance of various measurement techniques, α_B allows comparison of performance, independent of measurement technique.

For comparison purposes, it is useful to identify "typical" values of α_B for the different techniques. Spectral efficiencies can be difficult to estimate from the literature because spectral and temporal uncertainty are often specified separately. Some "typical" values are provided here. However, it should be remembered that these values, calculated from a variety of sources, are included only to roughly compare techniques. They do not necessarily represent the state of the art.

For the FA technique (extremum counting), α_B is limited by the fact that for $\langle\Delta\tau\rangle$ to be determined, at least two extrema must be present in the measurement spectrum. From Eq. (15), this means that the minimum DGD-bandwidth product must be $\langle\Delta\tau\rangle\Delta\omega = \pi$, giving an SNR of 1, so $\alpha_B = 1/\pi$, or 0.3. This value could be improved by the use of a different evaluation technique (such as analyzing multiple level crossings, as opposed to only peaks and valleys [34]).

In the case of a low-coherence interferometric measurement, or equivalently, the FA technique (with Fourier-transform evaluation), DGD resolution is limited by the coherence time T_c of the broadband source. Reference [12] describes an interferometric technique capable of a temporal resolution of 11 fs, and from plotted results, the full-width-half-maximum of the interferogram allows an estimate of the spectral width of the source as $\Delta\omega \approx 1.4 \times 10^{13}\mathrm{s}^{-1}$ (about 20 nm). Setting σ to 11×10^{-15} s, Eq. (20) yields an α_B of 6 for low-coherence interferometry or the Fourier-transformed FA technique.

Polarimetric techniques generally have their bandwidth efficiency limited by noise in the polarization-sensitive detection. Since $\Delta\theta/\Delta\omega$ is used as the measure of DGD, the noise on the $\Delta\theta$ measurement and the noise on the $\Delta\omega$ measurement both affect α_B. However, if a wavelength meter is used in the measurement, uncertainty on $\Delta\omega$ will be small, and $\delta\Delta\theta$ (the uncertainty in $\Delta\theta$) will dominate (for small values of $\Delta\tau$). With this assumption and Eq. (6), we find $\sigma = \delta\Delta\theta/\Delta\omega$. Combining this with Eq. (20) yields $\alpha_B = 1/\delta\Delta\theta$, the inverse of the Stokes noise. For comparison purposes, achievable values of α_B for a JME technique have been found informally to be ~ 850.

For RF phase-shift techniques, the measurement bandwidth is determined by the modulation frequency, and the measurement noise is fundamentally limited by the phase resolution $\Delta\varphi$ of the phase-sensitive detector (lockin amplifier, vector voltmeter, or network analyzer). Defining the DGD resolution as the time delay corresponding to the phase resolution, we find the bandwidth efficiency factor for RF phase-shift-based techniques to be

$$\alpha_B = \frac{360^\circ}{4\pi\Delta\varphi_{\mathrm{deg}}}, \tag{21}$$

where $\Delta\varphi_{\mathrm{deg}}$ is in degrees. Recently, an averaged MPS measurement reported an α_B of 3600 [30].

Finally, based on a specification sheet for a swept-wavelength system, the technique is expected to yield an uncertainty of 27 fs in a bandwidth of 50 pm or an uncertainty of 85 fs in a bandwidth of 10 pm. This gives an α_B of between 950 and 1500. The variation in α_B is likely due to a noise floor.

5. Wavelength Step Size

If spectral resolution and available bandwidth are not limiting factors, it is attractive to use a larger frequency step in the measurement to improve the DGD uncertainty. Since most frequency-domain measurement systems can easily vary the spectral resolution, it is important to be aware of the tradeoffs. For polarimetric techniques, which determine DGD through measurement of $\Delta\theta/\Delta\omega$, it is important to note that $\Delta\theta$ is known only to within a factor of 2π, and the determination of $\Delta\theta/\Delta\omega$ can suffer from aliasing if $\Delta\theta$ is greater than π for the given frequency step $\Delta\omega$. This has implications in all the frequency-domain measurement techniques, and can be expressed as the requirement that

$$\Delta\tau\Delta\omega \leq \pi, \tag{22}$$

or, in terms of wavelength, measurements cannot be trusted unless

$$\Delta\tau\Delta\lambda \leq 4 \text{ ps} \cdot \text{nm}, \tag{23}$$

where, for Eq. (23) only, $\Delta\tau$ is in units of picoseconds, $\Delta\lambda$ in nanometers, and a nominal operating wavelength of 1550 nm is assumed. In order to take into account variations in DGD with wavelength, $\Delta\tau$ in Eqs. (22) and (23) should represent the maximum DGD over the measurement range (not just the average). The need to resolve spectral variation in DGD requires a further increase in the spectral sampling density. Sufficient points must be measured to resolve the variations in DGD with wavelength. Multiple simulations on mode-coupled devices of various mean DGD values show that, due to the presence of second-order effects (wavelength-dependent DGD and PSP), the sampling density must be higher than for non-mode-coupled artifacts. Figure 14 shows that for a highly mode-coupled device, increased sample density improves the accuracy of the estimated mean DGD. For example, to measure a mean DGD that is $\sim 95\%$ of the true value, the sampling density must be such that

$$\Delta\tau\Delta\lambda \leq 1.5 \text{ ps} \cdot \text{nm}, \tag{24}$$

(at 1550 nm), where again $\Delta\tau$ is in picoseconds and $\Delta\lambda$ is in nanometers. This is a stricter requirement than the common expression in Eq. (23), and agrees well with the definition of the bandwidth of the principal states of polarization given by Jopson [35] as

$$\Delta\omega_{\text{PSP}} = \frac{\pi}{4\Delta\tau}. \tag{25}$$

6. Conclusion

In measuring PMD, the first choice to be made is deciding which measurement technique to use. Here, the various techniques have been described so as to illustrate their

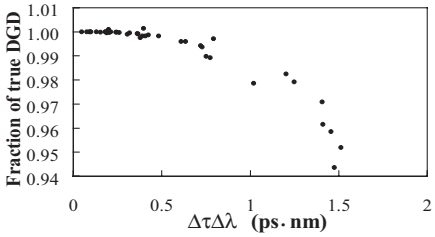

Fig. 14. Simulated results of measured DGD from a highly mode-coupled device as a function of sample density (vertical axis shows measured DGD normalized to true DGD).

relative merits. Generally, decisions are made based on measurement time, spectral resolution, and what quantities are measurable. Once a measurement technique is chosen, it is most important to understand the sources of measurement error (and to minimize them). The most significant of these sources have been described here.

References

[1] Paul A. Williams, "Mode-coupled artifact standard for polarization-mode dispersion: Design, assembly, and implementation," Appl. Opt., **38**, 6498–6507 (1999).

[2] N. Gisin, B. Gisin, J.P. Von der Weid, R. Passy, "How accurately can one measure a statistical quantity like polarization-mode dispersion?" IEEE Photon. Technol. Lett., **8**, 1671–1673 (1996).

[3] Dennis Derickson, *Fiber Optic Test and Measurement* (Prentice Hall, New Jersey, 1998).

[4] C.D. Poole, and C.R. Giles, "Polarization-dependent pulse compression and broadening due to polarization dispersion in dispersion-shifted fiber," Opt. Lett., **13**, 155–157 (1987).

[5] Yoshinori Namihira and Jun Maeda, "Polarization mode dispersion measurements in optical fibers," Technical Digest - Symposium on Optical Fiber Measurements, Boulder, 145–150 (1992).

[6] B. Bakhshi, J. Hansryd, P.A. Andrekson, J. Brentel, E. Kolltveit, B.K. Olsson, and M. Karlsson, "Measurement of the Differential Group Delay in Installed Optical Fibers Using Polarization Multiplexed Solitons," IEEE Phot. Tech. Lett., **11**, 593–595 (1999).

[7] Joseph W. Goodman, *Statistical Optics* (Wiley, New York, 1985), p. 168.

[8] B.L Heffner, "Influence of optical source characteristics on the measurement of polarization-mode dispersion of highly mode-coupled fibers," Opt. Lett., **21**, 113–115, (1996).

[9] P.A. Williams, "Accuracy issues in comparisons of time- and frequency-domain polarization mode dispersion measurements," Technical Digest—Symposium on Optical Fiber Measurements, Boulder, 125–129 (1996).

[10] TIA/EIA FOTP-124. 1999. Polarization-mode dispersion measurement for single-mode optical fibers by interferometric method. Telecommunications Industry Association, Arlington, VA.

[11] N. Cyr, "Polarization-Mode Dispersion Measurement: Generalization of the Interferometric Method to Any Coupling Regime,"J. Lightwave Technol., **22**, 794–805 (2004).

[12] Ph. Oberson, K. Julliard, N. Gisin, R. Passy, and JP Von der Weid, "Interferometric Polarization Mode Dispersion Measurements with Femtoseconds Sensitivity," Technical Digest—Symposium on Optical Fiber Measurements, Boulder, 143–146 (1996).

[13] N. Cyr, R. Roberge, J. Bradley, G. Amice, F. Audet, and G.W. Schinn, "Interferometric PMD Measurement of a Transatlantic 5512-km Fiber Link Including 119 EDFAs," Optical Fiber Communications Conference, Session MF, (2004).

[14] N. Cyr, Michel Leclerc and Bernard Ruchet, "PMD measurements in multipath components: The single waveplate example," Proceedings of Photonics North, Quebec (2002).

[15] P.A. Williams and J.D. Kofler, "Measurement and mitigation of multiple reflection effects on the Differential Group Delay Spectrum of optical components," Technical Digest—Symposium on Optical Fiber Measurement, Boulder, 173–176 (2002).

[16] C.D. Poole, N.S. Bergano, R.E. Wagner, and H.J. Schulte, "Polarization dispersion and principal states in a 147 km undersea lightwave cable," J. Lightwave Technol., **LT-7**, 1185–1190 (1989).

[17] B.L. Heffner, "Automated Measurement of Polarization Mode Dispersion Using Jones Matrix Eigenanalysis," IEEE Photon. Technol. Lett., **4**, 1066–1069 (1992).

[18] R.M. Jopson, "Measurement of Second-Order Polarization-Mode Dispersion Vectors in Optical Fibers," IEEE Photon. Technol. Lett., **11**, 1153–1155 (1999).

[19] N. Cyr, A. Girard, and G.W. Schinn, "Stokes Parameter Analysis Method, the Consolidated Test Method for PMD Measurements," Proceedings National Fiber Optics Engineers Conference, Chicago, 1999.

[20] TIA/EIA FOTP-122. 1999. Polarization-Mode Dispersion Measurement for Single-Mode Optical Fibers by Stokes Parameter Evaluation. Telecommunications Industry Association, Arlington, VA.

[21] R.C. Jones, "A New Calculus for the Treatment of Optical Systems: VI. Experimental Determination of the Matrix," J. Opt. Soc. Am., **37**, 110–112 (1946).

[22] J.K. Kofler and P.A. Williams, National Institute of Standards and Technology, unpublished.

[23] Mary L. Boas, *Mathematical Methods in the Physical Sciences* (Wiley, New York, 1983), p. 454.

[24] Craig D. Poole, "Polarization-Mode Dispersion Measurements Based on Transmission Spectra Through a Polarizer," J. Lightwave Technol., **12**, 917–929 (1994).

[25] P.A. Williams and C.M. Wang, "Corrections to Fixed Analyzer Measurements of Polarization Mode Dispersion," J. Lightwave Technol., **16**, 534–541 (1998).

[26] B.L. Heffner, "Single-mode propagation of mutual temporal coherence: equivalence of time and frequency measurement of polarization-mode dispersion," Opt. Lett., **19**, 1104–1106 (1994).

[27] P.A. Williams, A.J. Barlow, C. Mackechnie, and J.B. Schlager, "Narrowband measurements of polarization-mode dispersion using the modulation phase shift technique," Technical Digest—Symposium on Optical Fiber Measurements, Boulder, 23–26 (1998).

[28] P.A. Williams, "Modulation phase-shift measurement of PMD using only four launched polarization states: a new algorithm," Electron. Lett., **35**, 1578–1579 (1999).

[29] L.E. Nelson, R.M. Jopson, H. Kogelnik, and J.P. Gordon, "Measurement of polarization mode dispersion vectors using the polarization-dependent signal delay method," Opt. Express, **6**, 158–167 (2000).

[30] P.A. Williams and J.D. Kofler, "Narrowband Measurement of Differential Group Delay by a Six-State RF Phase-Shift Technique: 40 fs Single-Measurement Uncertainty," J. Lightwave Technol., **22**, 448–456 (2004).

[31] G.D. VanWiggeren, A.R. Motamedi, D.M. Baney, "Single-Scan Interferometric Component Analyzer," IEEE Photon. Technol. Lett., **15**, 263–265 (2003).

[32] G.D. VanWiggeren, and D.M. Baney, "Swept-Wavelength Interferometric Analysis of Multiport Components," IEEE Phtoton. Technol. Lett., **15**, 1267–1269 (2003).

[33] L.B. Jeunhomme, *Single-Mode Fiber Optics: Principles and Applications* (Marcel Dekker, New York, 1983), p. 66.

[34] A. Galtarossa, L. Palmieri, M. Schiano, and T. Tambosso, "Accuracy Enhanced PMD Measurements with Wavelength Scanning Technique," Technical Digest— Optical Fiber Measurement Conference, Nantes 45-48, (1999).

[35] R. Jopson, L. Nelson, and H. Kogelnik, "Measurement of second-order PMD vectors in optical fibers," IEEE Photon. Technol. Lett., **11**, 1153–1155 (1999).